Sedimentary Geology 275–276 (2012) 79–92

Contents lists available at SciVerse ScienceDirect

Sedimentary Geology

journal homepage: www.elsevier.com/locate/sedgeo

Preservation of forcing signals in shallow water carbonate sediments

Jon Hill [a,*], Rachel Wood [a,b], Andrew Curtis [a,b], Daniel M. Tetzlaff [c]

[a] Grant Institute, School of GeoSciences, University of Edinburgh, Kings Buildings, West Mains Road, Edinburgh, EH9 3JW, UK
[b] Edinburgh Collaborative of Subsurface Science and Engineering (ECOSSE), School of GeoSciences, University of Edinburgh, Kings Buildings, West Mains Road, Edinburgh, EH9 3JW, UK
[c] Schlumberger Information Solutions, 5599 San Felipe Ave., Suite 1700, Houston TX, 77056, USA

ARTICLE INFO

Article history:
Received 24 March 2012
Received in revised form 18 July 2012
Accepted 20 July 2012
Available online 1 August 2012

Editor: B. Jones

Keywords:
Carbonate sedimentation
Cyclicity
Forward modelling
Preservation
Spectral analysis

ABSTRACT

No consensus has been reached on whether the metre-scale cycles that commonly occur in peritidal carbonates are predominately a product of external relative sea-level variations (allocycles) or an intrinsic property of carbonate production generated via the interaction of non-linear processes (autocycles). For any forcing signal such as eustatic sea-level change, to be detectable in stratigraphy its effects must be preserved. Here, a deterministic, three-dimensional geological process model is used to explore how such cycles are preserved in the geological record in the presence of autocyclic processes. Each simulation produced cycle thickness distributions that are statistically indistinguishable from a theoretical Poisson process, regardless of whether auto- or allo-cycles dominated. Spectral analysis of depositional time series constructed from idealised geological sections showed that all detectable signals occurred within the Milankovitch forcing frequency bands, even when no Milankovitch forcing was present. Thus, it is deduced that from any geological section alone, external forcing signals are detectable but are not distinguishable from autocyclically produced signals. Interestingly, there is no correlation between the percentage of sediment preserved and the accuracy with which signals are detectable in the preserved sediment: in some model realisations, even with preservation as low as 40%, the correct forcing signal can be detected accurately while, conversely, sections with preservation as high as 90% can have poor signal preservation. The reverse can also be true in other models. It is therefore concluded that distinguishing allocyclic and autocyclic forcing in shallow marine or peritidal carbonate successions is likely to be extremely difficult except in cases of extraordinary sedimentary preservation and dating accuracy.

1. Introduction

The observation of metre-scale cycles (Fig. 1) is common in many ancient carbonates, most notably in peritidal settings (Ginsburg, 1971; Goldhammer et al., 1993). The actual facies recorded vary from fining upwards to coarsening upwards sequences (Spence and Tucker, 2007). The cause of flooding surfaces is an increase in relative water depth at a given location, which is due either to eustatic sea-level rise or to periods of non-deposition coupled with subsidence and/or erosion. Eustatic sea-level changes driven by orbital forcing (Milankovitch rhythms) are often given as the primary driver for the cyclicity observed in the rock record (e.g. Spalluto, 2011). Alternative explanations include tectonic forcing (Bosence et al., 2009) and as a result of autocyclic phenomena, whereby relative changes in sea-level are created by interactions of non-linear sedimentary processes intrinsic to carbonate production (Ginsburg, 1971). However, it is likely that a number of processes interact (Tucker and Garland, 2010).

The origin of carbonate cycles is of considerable importance. If cyclic accumulations can be demonstrated to be dominantly allocyclic and driven by glacio-eustatic forcing, then a high resolution, temporal framework exists within ancient deposits that would enable the measurement of sediment accumulation rates, evolution and correlation in unprecedented detail. If, by contrast, such successions are dominantly autocyclic then their distribution should rather be interpreted as informing models of interacting sedimentary processes (Drummond and Wilkinson, 1993). Alternatively, the relative sea-level changes recorded could be tectonic in origin and hence the cycles would record local tectonic histories (Bosence et al., 2009).

The forcing mechanisms have been inferred in a number of ways. Milankovitch forcing can control sediment deposition via eustatic sea-level change. They have been inferred via cycle stacking patterns with cycle thickness ratios of either 4:1 or 5:1 (100 kyr:25 kyr or 100 kyr:20 kyr) (e.g. Goldhammer et al., 1987, 1993; Decisneros and Vera, 1993; Balog et al., 1997; Bosence et al., 2000; Barnett et al., 2002; Hofmann et al., 2004) when two or more Milankovitch rhythms were operating or via spectral analysis using cycle thicknesses as a time series (e.g. Balog et al., 1997). Such spectra have frequencies of cycles per unit, so unless the time taken for cycles to form can be estimated, the time series cannot be converted into temporal frequencies (e.g. Hinnov and

* Corresponding author at: Department of Earth Science and Engineering, Imperial College London, London, SW7 2AZ, UK.
E-mail address: jon.hill@imperial.ac.uk (J. Hill).

0037-0738/$ – see front matter © 2012 Elsevier B.V. All rights reserved.
http://dx.doi.org/10.1016/j.sedgeo.2012.07.017

Fig. 1. Shallow marine ramp cycles in San Andres Formation, USA (Algerita Escarpment). The variation in cycle thicknesses can be seen clearly.

Goldhammer, 1991). Evidence for autocyclic controls comes mainly from statistical properties. Analysis of cycle thickness distributions from field data would show no significant differences from theoretical distributions assembled from stochastic Poisson processes (Wilkinson et al., 1998). The stochastic process manifests as an exponential decrease in frequency with increasing cycle thickness (Wilkinson et al., 1996, 1999) but this result is not ubiquitous in the geological record (Burgess, 2008; Burgess and Pollitt, 2012).

All forcing mechanisms can be understood via numerical forward modelling where knowledge of physical, chemical and biological processes is encoded into algorithms that can perform simulations of sedimentary deposition over geological timescales. A number of independent models have shown that autocycles can form from various interacting processes (Demicco, 1998; Burgess and Wright, 2003; Burgess and Emery, 2004; Burgess, 2006), even without recourse to random processes (Hill et al., 2009).

Ultimately, the rock record is incomplete (Sadler, 1981). Statistical and spectral analysis of peritidal carbonate field data potentially relies on questionable assumptions. The primary driving mechanisms is not known *a priori* and hence the sensitivity of various statistical tests to differentiate between stochastic processes or Milankovitch forcing is not well understood. Moreover, the preservation rate of sediments has an influence on which signals can be inferred or observed from the rock record, even in principle (Wheatcroft, 1990). The incompleteness of the rock record is given as the primary reason behind so-called "missed-beats" (Goldhammer et al., 1987). However, this then raises the question of how much of the sediment must be preserved in order for the analyses to detect correctly any influencing forcing signal with statistical significance. Without prior knowledge about the forcing signals, this question is impossible to answer from the rock record alone.

One method to study the interaction of forcing signal, non-linear internal processes, and cycle preservation in the geological record is numerical forward modelling. Such simulations can include a complete analysis of production, deposition, erosion and transport, and the relative influence of each process can be assessed. Several computer models have confirmed that realistic carbonate sedimentary sequences can be generated by various combinations of non-linear interacting processes that are capable of producing autocycles (Demicco, 1998; Burgess, 2001; Burgess and Wright, 2003; Hill et al., 2009). Moreover, forward models can produce patterns similar to those observed in the rock record under the influence of allocyclic sea-level forcings (Demicco, 1998; Burgess, 2006). Computer models have been used to explore the interaction of eustatic sea-level variation and autocyclic mechanisms (Burgess, 2006; Dexter et al., 2009; Burgess and Pollitt, 2012). However, all models are limited in terms of the type and number of processes that are included, so it is necessary to repeat such studies with several independent models.

Here it is shown how a numerical forward peritidal process model, Carbonate GPM (Hill et al., 2009), can generate metre-scale shallowing-upwards carbonate autocycles using purely physico-chemical controls. These form solely due to the interaction of the sedimentary processes with no additional randomness being imposed. This model is then used to test the effects of superimposed eustatic sea-level changes on the generated cyclicity.

The modelled stratigraphy generated by Carbonate GPM can be used to produce power spectra from three different data series: true water depth, preserved water depth, and cycle thickness changes. The last corresponds to data derived from field studies, and the preserved water depth history represents the "best case" scenario in which it is assumed the water depth can be derived accurately from the preserved sediments. The true water depth provides a complete record of both external and internal forcings and would be identical to the preserved water depth in the case of a geological stratigraphy that is temporally complete. It is shown that the power spectra derived from preserved water depth history and cycle thickness changes do not match those derived from true water depth changes under a range of different forcing frequencies and amplitudes. The large range of apparent frequencies observed leads us to infer that, given our understanding of carbonate deposition and preservation, any direct statistical analysis of apparent cycle timings is at best questionable.

2. Methods

In order to obtain data to assess the relative influence of preservation and forcings on signals derived from shallow water carbonate cycles the finite-difference, numerical forward model, Carbonate GPM (Hill et al., 2009) was used. Multiple simulations were carried out driven by sea-level changes varying at single or multiple periods of oscillation, and across a range of amplitudes. From each of these simulations diagnostic quantities were derived at each location in the model from which a spectral analysis could be performed to determine which signals were preserved in the simulated rock record. Coupling these diagnostic quantities with knowledge of the percentage of rock preservation in the record, the effect of preservation and erosion of sediment on data observable in the field can be determined.

2.1. Carbonate GPM

Carbonate GPM (Hill et al., 2009) is a 3D numerical forward process model simulating geological processes forward in time, and is derived from the model GPM (Tetzlaff and Priddy, 2001). As such it inherits all processes of erosion, deposition, wave action, compaction, fault activity, fluctuating sea-level, siliciclastic sediment sources, and flow regimes from that model. Carbonate sediments have been modelled by incorporating in-situ carbonate production with growth rates based on environmental parameters at each location in the model. No random processes occur—the model is fully deterministic. The model simulates two carbonate types, reef and non-reef. Reef material is relatively more resistant to erosion than non-reef. The model starts from a given antecedent topography (Fig. 2a) and records the amount of sediment deposited at each location at each of a series of short timesteps. Every 2500 yr a surface is drawn at the top of the sediment at that point in time, thereby recording the sedimentary stratigraphy (Fig. 2b).

Carbonate GPM is unique in that it modifies carbonate production rates based on carbonate supersaturation via a proxy of residence time of water in the lagoon area (Demicco and Hardie, 2002). In addition, light attenuation and wave energy also affect carbonate growth rates. The model uses the same schema as several other forward models by defining a maximum carbonate production rate and reducing this according to local environmental factors (e.g. Bosscher and Schlager, 1992; Burgess, 2001; Warrlich et al., 2002). For both reef and non-reef sediments *c*,

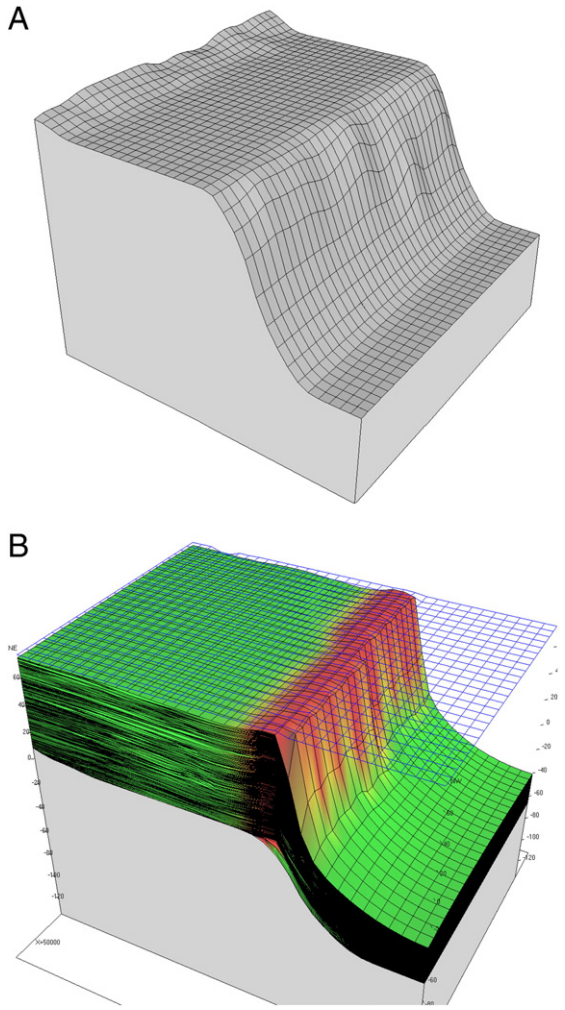

Fig. 2. Initial topography (A) and example output (B) from Carbonate GPM. In the example output green denotes non-reef sediment, red denotes reef sediment. The blue grid shows current sea-level. Time lines (in black) are drawn every 2500 yr to show simulated stratigraphy.

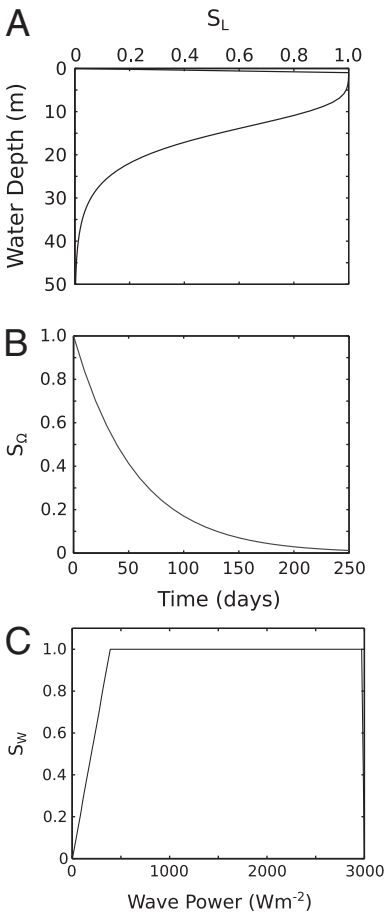

Fig. 3. Stress functions used to control local carbonate precipitation rates. A) S_L: depth-dependent function. B) S_Ω: residence time dependent function. C) S_W: wave power dependent function. See main text for details.

and at each point in time t, and surface position x, production P [m/yr] is calculated using:

$$P\left(\underline{x}, c, t\right) = S_L(L, c, t) \cdot S_\Omega(\Omega, c, t) \cdot S_W(W, c, t) \cdot P_m(c) \quad (1)$$

where the various terms labelled S are so-called stress functions (taking values between 0 and 1) that define the production efficiency decrease caused by various controlling environmental factors relative to the maximum production rate for each type of carbonate, $P_m(c)$ [m/yr]. Controlling factors on which the stress functions depend are water depth as this controls light availability (L), carbonate supersaturation (Ω) and wave energy (W), through the individual stress functions, S_L, S_Ω and S_W respectively.

The form of the individual stress functions (Fig. 3) controls the rate of carbonate precipitation as a function of environmental conditions. For example, reef-type sedimentary deposition is highest where wave energy is greatest, whereas non-reef-type sediments are deposited in less energetic water. S_L imposes an exponential increase of production rate with decreasing water depth (Fig. 3a) but with an additional linear decrease in the top one metre of water which represents the near-surface influence of tidal variations. S_Ω is derived from a proxy for carbonate supersaturation in lagoonal waters, namely water residence time (Ω) (Fig. 3b). The residence time for a parcel of water is a measure of how long that parcel has been isolated from open marine water; longer isolation leads to fewer carbonate ions contained in that parcel due to previous carbonate precipitation along the parcel's path. The form of this stress function is based on the results of Demicco and Hardie (2002) where the residence time and local supersaturation of water were measured across the Bahama Banks to define their functional relationship. In Carbonate GPM the residence time of every "parcel" of water is tracked from the point at which it enters the lagoon from the open ocean and from this spatially varying, local supersaturation can be inferred across the lagoon. The inclusion of residence time as a control on carbonate production gives an implicit lag time between sediment deposition ceasing due to high residence time or exposure and sedimentation recommencing. The sediment deposition cannot recommence until residence time in the area is below the threshold shown in Fig. 3b. Finally, S_W is the stress function based on wave power dissipation (W) (Fig. 3c). Carbonate GPM can model any number of wave sources, each with a defined wave period, amplitude and position. Here, a line source is used across the open marine boundary which produces waves that travel perpendicular to the shoreline. The wave energy is dissipated as the waves break in shallow water. The shape of the curve in Fig. 3c is based on measurements of growth rates and wave energy from modern reef sediments. Full details of the derivation of the stress functions and the algorithms incorporated into Carbonate GPM are given in Hill et al. (2009).

2.2. Experiments and diagnostics

Each simulation of the model commences from a simple platform antecedent shelf-edge topography (Fig. 2a). The platform is square in

plan view, of size 50×50 km, represented by a square grid of 35 cells on each side. The initial basin floor is 70 m below the platform and a smooth slope connects the basin floor to the top of the platform. Various model parameters used are given in Table 1. The baseline simulation (simulation 1) has no periodic signal enforced, but a constant subsidence rate of 100.0 m/Myr creates accommodation space. In subsequent simulations five different sinusoidal, eustatic sea-level changes are imposed upon the initial simulation. The oscillations of these sea-level changes fall into the expected frequency and amplitude ranges of so-called fifth and fourth-order cycles. This study therefore limits itself to examining processes within the range of eustatic variations thought to be indicative of Milankovitch forcing (Goldhammer et al., 1993). This results in six model simulations in total (Table 2) from which the results below were inferred.

From each simulation three diagnostic variables are calculated at each cell location in the area between the reef and shoreline. This gives a total of 630 vertical sections from each simulation. The diagnostics calculated and used in subsequent analyses are: the true water depth history, preserved water depth history, and the cycle thicknesses. The true water depth is constructed by sampling the simulated water depth at each location every 2500 yr of simulated time. As such, this is actually the water depth experienced at that geographical location, irrespective of how much sediment is preserved, and is therefore a record of the true relative sea-level curve at each location. This diagnostic is equivalent to a rock sequence that has 100% preservation from which accurate water depths and ages can be determined. The preserved water depth diagnostic is calculated from the true water depth curve from each point by removing those sections that are not preserved in the final stratigraphy due to erosion or non-deposition. Missing data are then interpolated using a cubic spline to provide a time series of the same length as the true water depth curve. This diagnostic is equivalent to a rock section from which accurate water depths can be determined from preserved parts of the geological record and where missing parts of the section can be detected and the time interval of the resulting unconformity can be determined. The final diagnostic is the cycle thickness variation through time. In order to define each cycle the timing of hiatus events was recorded for each location. The amount of sediment deposited between two hiatus events is defined to constitute one cycle, assuming a shallowing of water depth towards the top of the cycle. This diagnostic is the closest possible modelled representation of real stratigraphic cycle data obtainable from the rock record that is afforded by Carbonate GPM. Assuming a constant subsidence rate of 100 m/Myr through time, the cycle thickness data can be converted to temporal range of each cycle. Note that this conversion is more accurate than that obtained from field data, which can have error margins of over 50% in assumed temporal ranges (e.g. Hinnov and Goldhammer, 1991) as in practise the average subsidence rate must itself be estimated.

Table 1
Summary of model parameters used in all simulations described here.

Parameter	Value
Display time	2500 yr
Diffusion coefficient	1000 m^2/yr (varying with depth)
Transport coefficient	10 s/m
Timestep	1 yr
Reef sediment grain size	15 mm
Non-reef sediment grain size	0.25 mm
Maximum reef production rate	3 mm/yr
Maximum non-reef production rate	2 mm/yr
Wave source amplitude	0.25 m
Wave source period	3.2 s
Wave direction	Perpendicular to shore
Cell dimensions	1470.6×1470.6 m
Model size	50×50 km (35×35 cells)

Table 2
Forcing frequencies and amplitudes for all simulations carried out here.

Simulation	Period	Amplitude
1	–	–
2	15 kyr	1 m
3	25 kyr	0.25 m
4	25 kyr	1 m
5	100 kyr	10 m
6	25 kyr and 100 kyr	1 m and 10 m

The three diagnostic variables are used to assess whether any external forcing signal might be detected. A maximum entropy spectral analysis (MESA) was performed for each diagnostic variable over all 630 vertical sections in the shore-to-reef area. MESA assumes that the time series conforms to an autoregressive model of order, p, i.e. the current value is a linear combination of the last p previous values, along with uncorrelated noise. The Fourier transform of the time series is used as the basis of the maximum entropy spectral estimator and then there are various formulations of the predictor-error filter. More details can be found in Kay and Marple (1981). MESA has been shown to perform better on field studies than more traditional spectral techniques (Hinnov and Goldhammer, 1991). The program MAXENPER (Pardo-Igzquiza and Rodriguez-Tovar, 2005) was used to carry out MESA analysis. In order to assess the significance of peaks found in the power spectra, a permutation test as described in Pardo-Igzquiza and Rodriguez-Tovar (2005) was carried out, which allows the significance of the spectral peaks detected to be calculated. This test creates random permutations of the data, assuming a white or red noise model, and from these permutations maximum entropy power spectra are generated. A total of 10,000 permutations were used for each location, along with a white noise model in this study.

One final diagnostic variable was calculated for each cell location—the percentage of sediment preserved. This was calculated using the ratio of the lengths of the true and preserved water depth sections, prior to interpolation of the preserved water depth data.

3. Results

3.1. Stratigraphic geometry

All stratigraphies show numerous hiatus events, indicated by bunching and bifurcation of timelines (Fig. 4). Bunching of timelines occurs when little net sediment is deposited in a locality causing the timelines to become spaced closer together. When the net deposition rate is zero (a hiatus), the timelines are exactly drawn on top of each other. Bifurcation of timelines occurs when deposition halts in one locality, but is continuing in neighbouring localities; this causes the timeline to split or join as it is tracked along a cross section. These changes in depositional rate throughout a simulation can be interpreted as cycles just as they are in field data: sedimentation will commence until the depth is too shallow or residence time is too high for carbonate production, after which a hiatus event occurs. Each hiatus event is particular to the environment at the time, so they vary in spatial and temporal extent. Following the hiatus a new shallowing upward cycle is formed: subsidence increases water depth until such time that sufficient water depth has been attained for production to re-commence (assuming all other controlling parameters are conducive to carbonate production). In the stratigraphic output this is indicated by the bunching of timelines as sedimentation rate slows in the uppermost part of the cycle, followed by several timelines occurring at the same stratigraphic level, indicating a hiatus in deposition. These timelines record the migration of depocentres around the lagoon, which is a large inter- and sub-tidal area, effectively modelling the migration of tidal islands in peritidal settings.

The stratigraphy produced by low amplitude fifth-order sea-level oscillations (Fig. 4, simulations 2–4) shows many similarities with

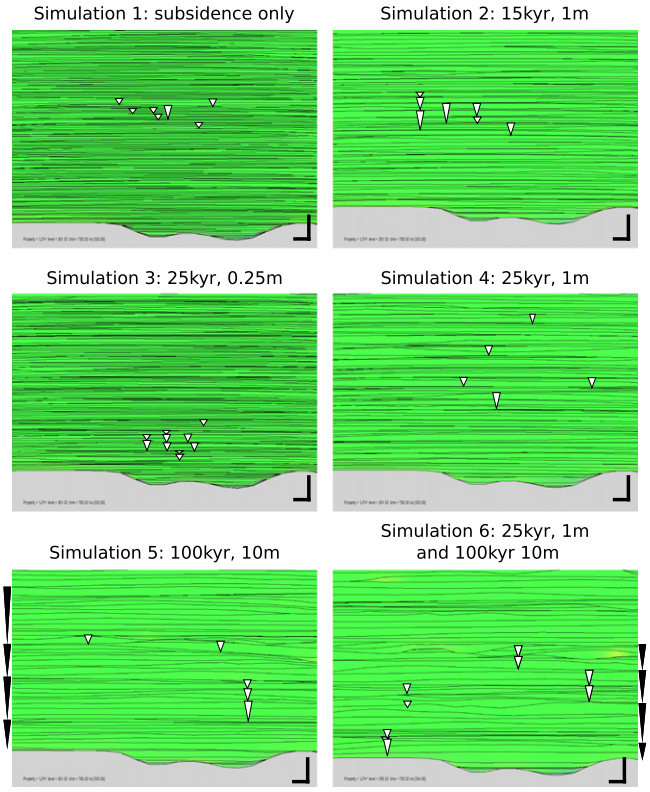

Fig. 4. Lateral cross-shore sections from all simulations. Cross sections are taken parallel to the reef, at the initial shoreline. Timelines (black lines) are drawn every 2500 yr. Where these bunch together little or no sediment is deposited. Black triangle (side of simulations 5 and 6) indicates clearly identified 100 kyr cycles (simulations 5 and 6 only). White triangles indicate high-frequency cycles. Note that these are not laterally continuous, so the symbols are placed where the cycle can be identified clearly. Only a small proportion of the many identifiable cycles are marked for illustration. Black bars for scale are 1.5 km in the horizontal direction and 2 m in the vertical direction for all sections.

the baseline simulation (Fig. 4, simulation 1). Hiatal events are not laterally continuous across the cross section and cycles vary between the individual vertical sections. There is little indication of a clear stacking pattern where several short cycles can be grouped into longer cycles. By contrast, higher amplitude, high-frequency oscillations of sea-level change, in conjunction with lower frequency changes result in more laterally extensive hiatal horizons across the platform, where several timelines occur at the same location in the stratigraphy (Fig. 4, simulations 5 and 6). Timelines run uninterrupted for up to 25 km before being cross-cut by later timelines or merging with earlier timelines. These features are caused by extensive exposure of the carbonate platform during lowstands. This is particularly clear in the back reef region, shown in Fig. 4, where clear cycles can be seen that visually correspond to the eustatic signal. These spatially extensive cycles can be interpreted as the 4th-order stratigraphic cycles seen in the rock record. Within these extensive cycles, several temporally and spatially less extensive sub-cycles can be found, much like the hierarchical stacking patterns seen in the rock record (e.g. Goldhammer et al., 1990; Satterley, 1996).

3.2. Cycle thickness distribution

Since all six simulations produced identifiable cycles, it is possible to determine whether the statistical techniques used in previous studies are sufficiently sensitive to distinguish between data that are purely autocyclic (simulation 1), a mixture of autocyclic and weakly forced (low amplitude) allocyclic cycles (simulations 2–4), and those that are a mixture of autocyclic and strongly forced (high amplitude) allocyclic cycles (simulations 5 and 6).

Fig. 5 shows cycle thickness distributions from each simulation. Drummond and Wilkinson (1993, 1996) proposed that the thickness distributions followed an exponential distribution, given by:

$$F = NB\ P\ e^{-PT} \tag{2}$$

where F is the frequency at a particular unit size, $P = N/L$, B is the bin size (here, 0.1 m, where a bin is a range of numerical value into which data are sorted), L is the total vertical length of the succession, and N is the number of cycles present. This theoretical distribution is shown in all cases as a straight line in Fig. 5.

The data from all simulations showed a correlation coefficient of 0.89 or greater when correlated against the theoretical distribution (Eq. (2)), and moreover, none showed a statistically significant (at the 99% confidence level) different from the theoretical distribution (Eq. (2)) using a Kolmogorov–Smirnov (K–S) test, which makes no assumptions about the distribution of the data (Burgess, 2008; Burgess and Pollitt, 2012). Dexter et al. (2009) showed that bin size has a significant effect on the correlation coefficient. Thus in order to check the robustness of this result, bin sizes ranging from 0.1 to 0.5 m were tested. There is an increase in correlation coefficients with increasing bin size, but unlike in the study of Dexter et al. (2009), all simulations here show correlation coefficients greater than 0.89 (Table 3). In addition, there appears to be no relationship with preservation percentage, with simulations that preserve only 43% of the total sediment deposited still showing very high correlation coefficients and being statistically indistinguishable from the theoretical distribution, regardless of bin size (Table 3). It is concluded that either the simulated thicknesses show an exponential distribution or that the K–S test is not sufficiently sensitive to detect deviations from that distribution.

3.3. Power spectra

Power spectra were generated from three different time series: true water depth curves, preserved water depth curves, and cycle thicknesses (Fig. 6). Each of these power spectra were generated for each cell in the model output within the shallow water area (630 cells). Using MENXPR, only statistically significant peaks were analysed. The spectra generated were converted from a "per unit" frequency scale to a time-based frequency, using the average cycle thickness and the exactly known subsidence rate. The significance of each peak is assessed using the method described above and is detailed in Pardo-Igzquiza and Rodriguez-Tovar (2005). All six simulations showed a range of frequencies at which statistically significant peaks occurred.

Figs. 6 and 7 show examples of the three types of spectra generated for each simulation taken from a point at the centre of the lagoonal area. Statistically significant spectral peaks (grey bands in Figs. 6 and 7) occur in all spectra, across all simulations. Generally, a larger number of significant peaks occur in spectra based on water depths, both preserved and true, than in those generated from cycle thickness histories. Where external eustatic forcing is present, it can be detected by the spectral analysis in the majority of cases; however, the correct peak is often amongst a number of other, equally strong, peaks.

The forcing signal is not always detected in the preserved water depth spectra, and is almost never detected accurately in the cycle thickness spectra, the nearest equivalent to typical field data. For example, the baseline simulation (simulation 1), which has no external forcing signal imposed, shows as many significant spectral peaks as the other simulations. It is concluded that without some form of prior knowledge about forcing imposed, it would be impossible to pick out the spectral peaks that correspond to a true forcing signal, even given a perfect temporal succession of water depth. This is therefore a fundamental constraint on what can be inferred from field data, and it can not be improved by better quality (more accurate) data.

In an attempt to understand the overall pattern of frequency detection, the number of occurrences of significant spectral peaks was counted

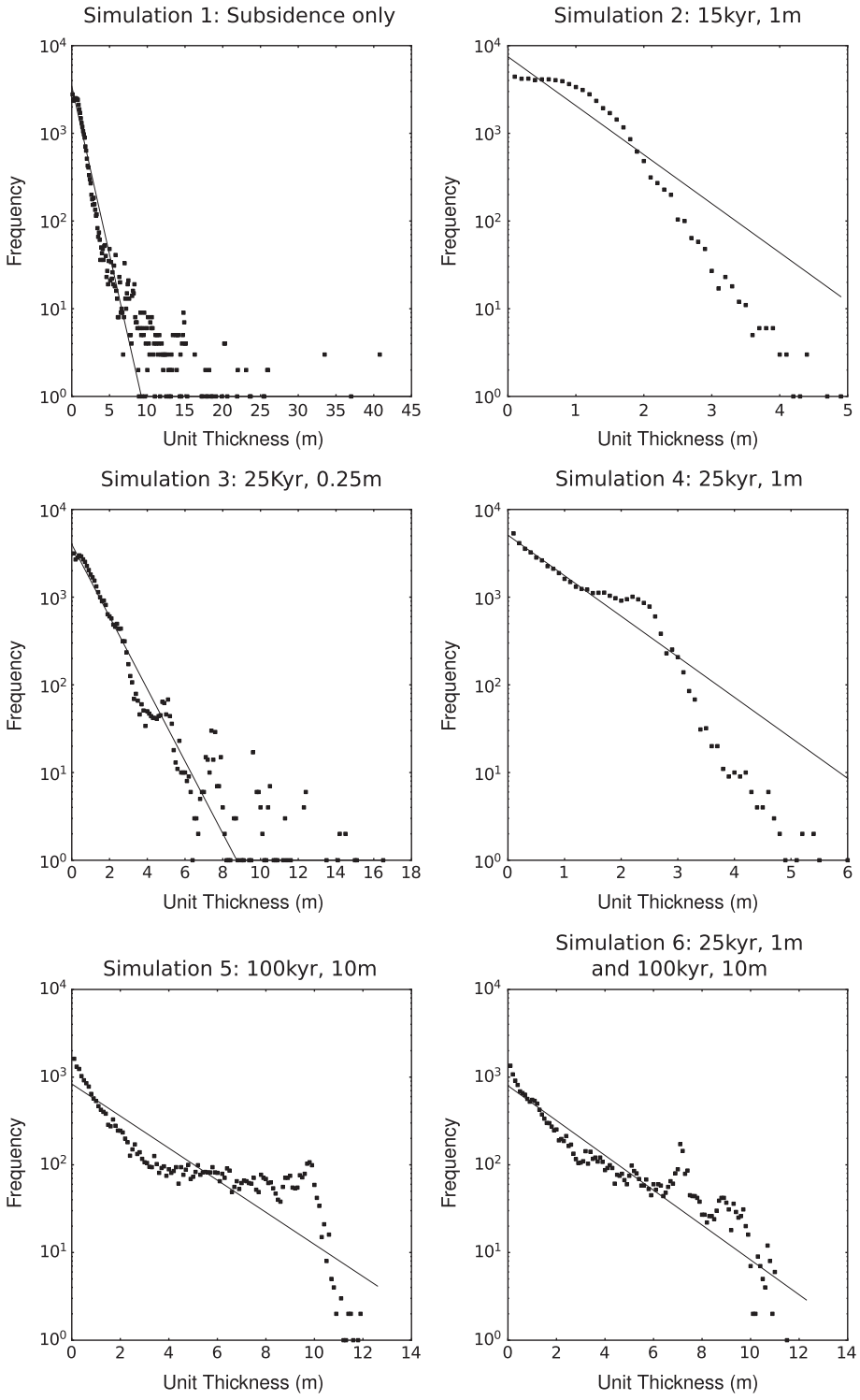

Fig. 5. Cycle thickness distributions from all six simulations. All are statistically indistinguishable from exponential distributions (straight lines) using identical tests to Drummond and Wilkinson (1996) and Burgess (2008).

for each simulation and for each diagnostic time series (Fig. 8). Generally, the spectra derived from the preserved water depth curves have higher counts of significant peaks (the dotted line is usually above the solid line in Fig. 8), especially at lower frequencies. Only simulation 6 did not show this trend. For simulations 2–6, in which a eustatic sea-level variation was imposed, the forcing frequency was recorded at a large number of locations. However, again it is seen that statistically significant spectral peaks are also recorded at a many frequencies other than the forcing frequency. This is interpreted to be due to autocyclic processes. In simulation 3 it is difficult to determine which of the frequently occurring spectral peaks is the imposed forcing signal because of the number of significant spectral peaks. This difficulty is attributed to the swamping of the eustatic signal by autocyclic processes. Compared to simulation 3, simulations 2 and 4 both showed a large increase in locations, where a significant spectral peak was detected at the forcing frequency, but with some leakage into neighbouring frequencies.

Table 3
Correlation coefficients of simulated cycle thickness distributions and theoretical distribution based on a Poisson process of cycle formation along with maximum, minimum and average preservation percentages.

Simulation	Bin size (m)								Pres. %		
	0.1	0.2	0.3	0.4	0.5	0.6	0.7	0.8	Max	Min	Av.
1	0.981	0.981	0.982	0.984	0.985	0.988	0.991	0.995	0.97	0.48	0.73
2	0.923	0.924	0.927	0.931	0.935	0.944	0.956	0.966	0.68	0.49	0.58
3	0.987	0.988	0.988	0.990	0.993	0.995	0.997	0.998	0.96	0.50	0.71
4	0.985	0.987	0.989	0.989	0.989	0.990	0.991	0.991	0.70	0.49	0.59
5	0.897	0.899	0.900	0.903	0.907	0.909	0.911	0.914	0.63	0.37	0.45
6	0.943	0.945	0.949	0.952	0.956	0.959	0.961	0.964	0.63	0.32	0.43

When including lower frequency forcing, both simulations 5 and 6 showed an increase in significant peaks around the forcing frequency, and harmonics thereof, for the true water depth curves. Harmonics are also present in simulations 2 and 4, though to a lesser extent. The harmonics are likely caused by the interaction of the two forcing frequencies (simulation 6) or the interaction of the forcing signal with incomplete sections. Both simulations 5 and 6 show a marked increase in the significant spectral count in both the preserved water depth and true water depth spectra at the forcing frequency. However, simulation 6 only shows a minor increase in the number of locations recording a significant spectral peak at the higher frequency but only in the spectra derived from true water depths.

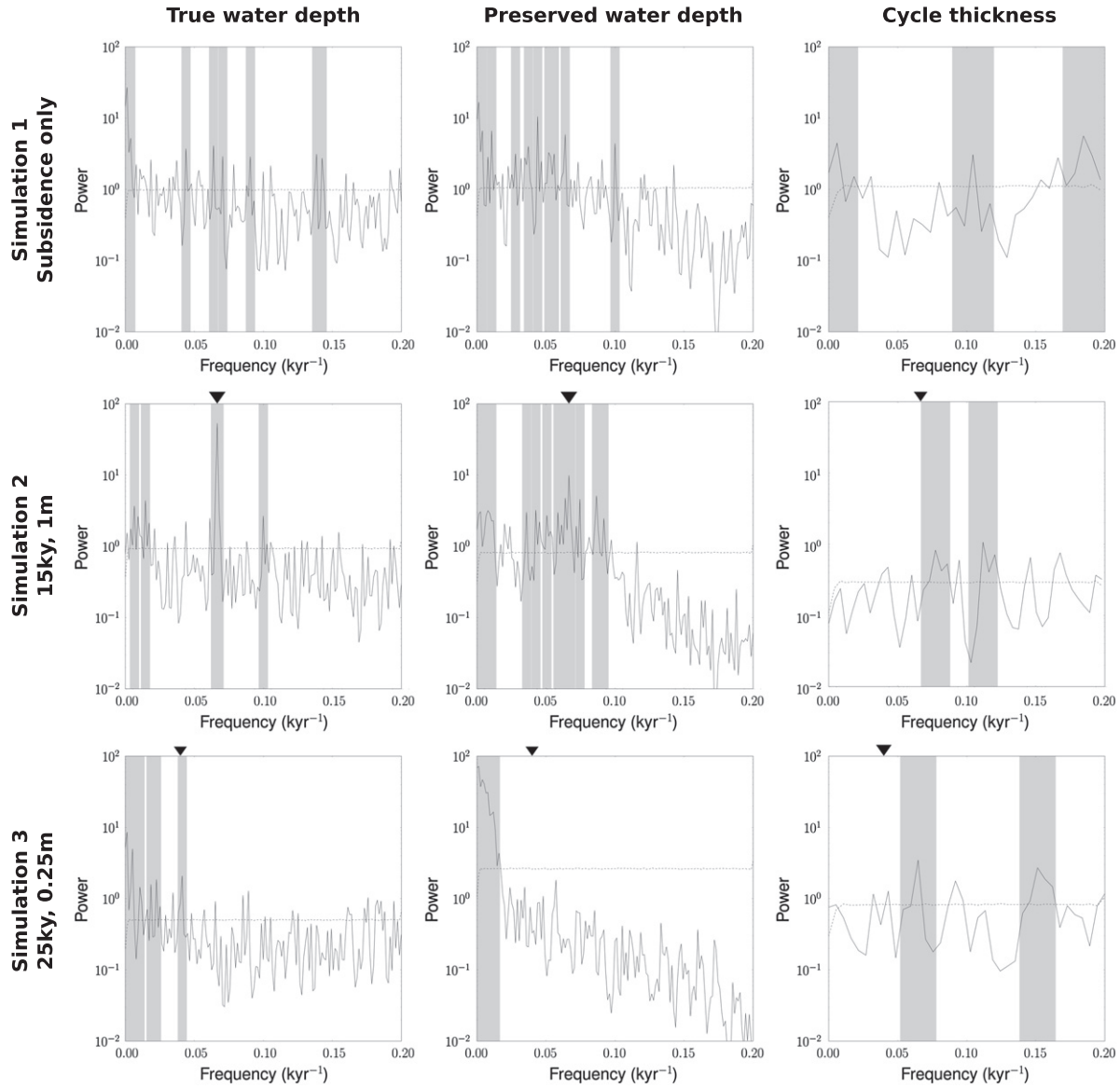

Fig. 6. Example power spectra from simulations 1 to 3 for all three data types. Significant peaks are highlighted by grey shading. Dotted line shows the average spectrum using a white noise model to determine significant peaks from 10,000 realisations. Black triangles on the upper axes indicate the forcing signal imposed, if any.

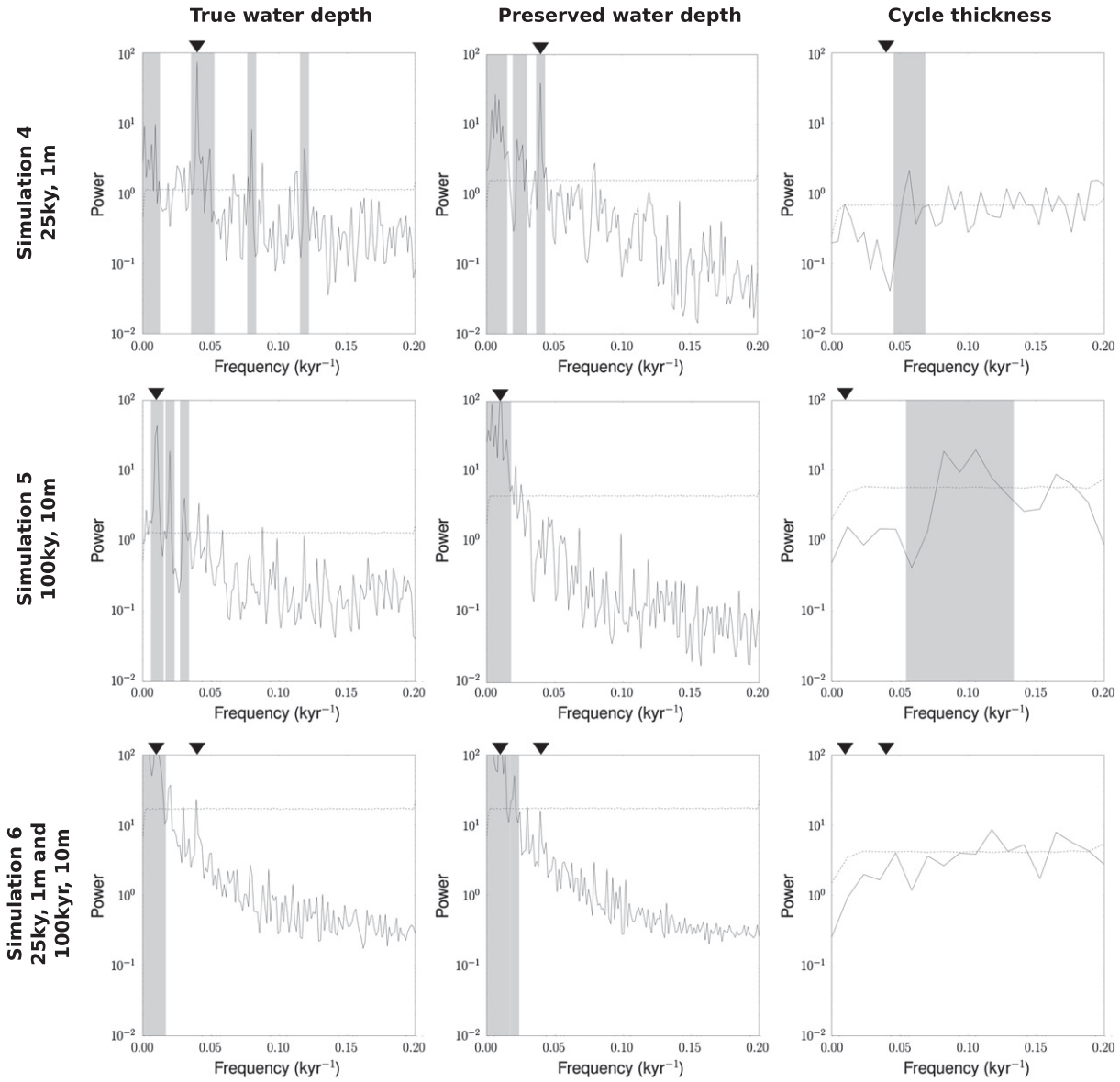

Fig. 7. Example power spectra from simulation 4 to 6 for all three data types. Significant peaks are highlighted by grey shading. Dotted line shows the average spectrum using a white noise model to determine significant peaks from 10,000 realisations. Black triangles on the upper axes indicate the forcing signal imposed, if any.

For all simulations the number of significant peaks found in the cycle thickness power spectra is significantly lower than that found using the other two diagnostic variables (Fig. 8). No simulation shows an increase in the number of locations at which significant peaks at the imposed forcing frequencies are found. However, multiple locations showed cycles at Milankovitch-scale frequencies, even in the baseline simulation where no forcing was used. Overall the cycle thickness spectra provided relatively poor data compared to the other two spectra; however, taken in isolation they would still constitute apparent evidence for Milankovitch-style forcing as most significant spectral peaks occur within the Milankovitch forcing frequency band.

Examining the different type of spectra together shows interaction of autocyclic and external forcing signals well. For example the baseline simulation (no forcing) showed multiple cells with spectral peaks at around 187 kyr and 107 kyr (0.00534 and 0.00934 1/kyr respectively), along with less common peaks between 20 (0.05 1/kyr) and 30 kyr (0.033 1/kyr) (Fig. 8). These are all within the Milankovitch forcing frequencies, yet no forcing was applied to this simulation. Simulation 2 shows a clear spectral peak at 15 kyr (0.0667 1/kyr) as expected in most locations, with some leakage into nearby frequencies. There are also significant peaks in a number of locations at around 150 kyr (0.00667 1/kyr), similar to the baseline simulation. Simulation 3 resembles the baseline most closely, but with a small increase in the number of peaks around 25 kyr (0.04 1/kyr), in around a sixth of all possible locations (around 105 of 630 cells). The dominant frequency seen in simulation 4 is 25 kyr (0.04 1/kyr) as expected (Fig. 8). Again, there are multiple locations that show peaks around 150 kyr (0.00667 1/kyr). Simulations 5 and 6 are very similar with both showing clear peaks at 100 kyr (0.01 1/kyr) as expected in the majority of locations. Simulation 6 did not have many locations that showed a peak at 25 kyr—the second forcing frequency, indicating that the lower amplitude, higher frequency signal is somewhat masked by the high amplitude, low frequency signal.

Of course a key question is how well spectral peaks from preserved data correspond to the spectral peaks from true water history. For each simulation, the number of locations where the preserved and cycle thickness spectra contained the same significant spectral peak as the spectrum generated from the true water depth curve was calculated and plotted as "Matches" in Fig. 9. In addition, the number of locations where a significant spectral peak in the preserved or cycle thickness spectra did not

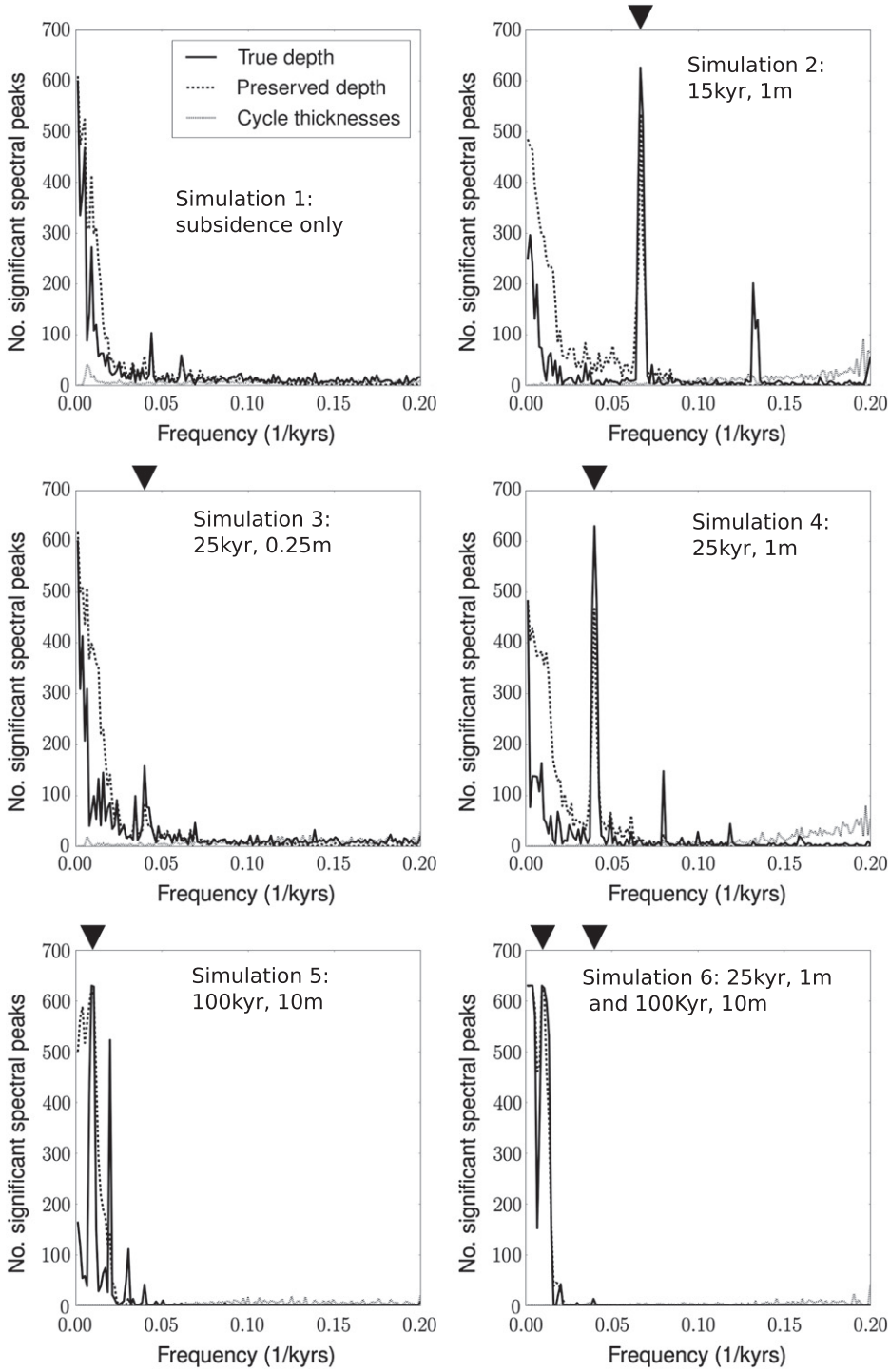

Fig. 8. Counts over all locations of significant spectral peaks occurring across all frequency bands. Black triangles indicate the forcing signal imposed. Plot titles give simulation name and the period and amplitude of the forcing signal.

match a significant peak in the true water depth spectra was also recorded ("Non-matches" in Fig. 9). Across all frequencies the number of non-matching peaks is generally higher than the number of locations with matching peaks for the preserved water depth spectra. For simulations 2, 4 and 5 there is a significant increase in the number of matches and a decrease in the number of non-matches at the forcing frequency—implying that the preserved water depth spectra are capable of detecting the forcing frequency. Simulation 6 shows that the 100 kyr signal was detected, but the 25 kyr signal was not. However, the true water depth spectra did not detect this signal well either. The number of matches between the true water depth spectra and cycle thickness spectra is very low, with no consistent pattern across frequencies. This is likely to be due to the lack of significant peaks in the cycle thickness spectra compared to the other two spectra.

Table 4 shows the number of matches and non-matches for all simulations. For all simulations, the spectra derived from cycle thicknesses showed far fewer matches than those from the preserved water depth curves. For simulations 5 and 6, where high amplitude forcing was present, the number of matching peaks was extremely low. However, all simulations bar simulation 6 showed more spectral peaks in

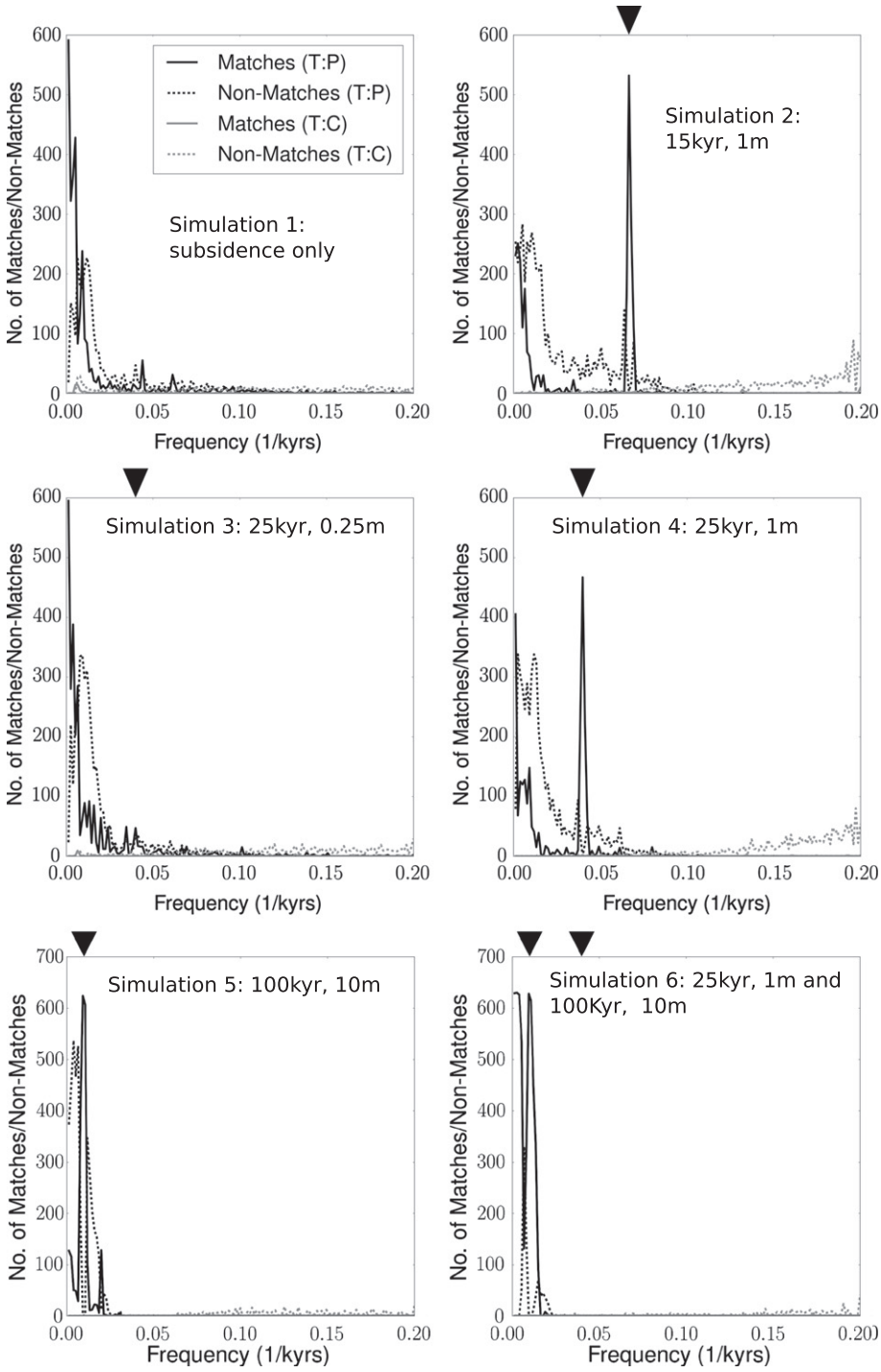

Fig. 9. Matches (solid) and non-matches (dotted) (see text for definitions) over all locations of significant spectral peaks across all frequency bands. Black triangles indicate the forcing signal imposed.

the preserved sections that did not occur in the true water depth sections. The same is true for spectra derived from cycle thicknesses: a higher number of significant peaks in the cycle spectra did not match equivalent peaks in the true water depth spectra than did match.

In addition to examining the frequencies at which significant peaks occurred, whether spectra derived from the three different data sources were statistically different was also examined. Using the Kolmogorov–Smirnov (K–S) test, which makes no assumptions about the distribution of the data, for each location, the *p*-value from the K–S test between the spectrum derived from the true water depth curve and the preserved water depth curve, and between the true water depth curve and the cycle thickness data, was calculated and plotted against sediment preservation percentage (Figs. 10 and 11). The underlying assumption here is that the true water depth spectra represent the correct signal, whereas the spectra from preserved water depth and cycles might be extracted from the rock record. A high similarity (i.e. the null hypothesis that the two records are from the same distribution cannot be rejected) will occur between the true water depth spectra and one of the other two types of spectra where the peaks match. Correspondingly, a low similarity (rejection of the null hypothesis) will occur where the peaks are

Table 4
Number of significant spectral peaks from the preserved water depth spectra and cycle thickness spectra that match the peaks in true water depth spectra (second and third column). Columns four and five show the number of significant peaks that did not match the forcing frequency imposed on the simulation. The last three columns show the total number of significant spectral peaks for each data source.

	No. matches		No. non-matches		Total sig. peaks		
Simulation	True:Pres.	True:Cycles	True:Pres.	True:Cycles	True	Pres.	Cycles
1	1748	53	2787	953	3280	4535	1006
2	1774	38	4470	1648	3841	6244	1686
3	1573	41	3642	1103	3450	5215	1144
4	1813	13	4273	1651	3605	6086	1664
5	2029	0	2571	603	3034	4600	603
6	5009	4	806	465	5597	5818	469

significantly different. Plotting the *p*-value against the preservation percentage will therefore reveal if the preservation percentage of sediment has any bearing on how well the two geological spectra preserve the signal of water depth changes. That is, it will detect whether the similarity of the power spectra is high where sediment preservation percentage is higher. A cut off at the 95% confidence level of the rejection of the null hypothesis of the two spectra being drawn from the same distribution is shown in Figs. 10 and 11 and the number of locations above and below this cut-off is detailed in Table 5.

The comparison between true water depth generated spectra and preserved water depth generated spectra shows a number of notable features (Fig. 10). First, when autocyclic processes dominate (simulations 1 and 3), the *p*-value varies from near zero to unity, but with a wide spread across the preservation percentage, with perhaps a slight trend of lower preservation percentage giving more confidence that the true and preserved spectra are equivalent. In contrast, simulations with an imposed sea-level forcing amplitude of a metre or more show a distinct banding within which the preservation percentage is constrained. This is to be expected as eustatic sea-level variations will naturally constrain the upper level of the preservation percentage. Simulations 2 and 4 (which were forced with a 1 m amplitude with 15 or 25 kyr period) show very few points where the null hypothesis can be rejected (Table 5). Simulation 5 shows more locations that have spectra that are significantly different than simulation 6; simulation 6 has fewer than one third of locations where the two spectra are not significantly different. The likely cause of this difference is the interaction of two forcing frequencies.

When carrying out the same analysis using the spectra derived from cycle thicknesses, all but simulation 6 show far fewer locations where the null hypothesis cannot be rejected (Fig. 11 and Table 5). Again, simulations 1 and 3 show slight trends where lower preservation percentage means a lower *p*-value. From Fig. 11 and Table 5 it is inferred that it is not the proportion of sediment preserved that is the controlling factor on whether a signal is preserved as otherwise would be expected a clear linear trend of increasing signal detection (correlation coefficient) with increasing preservation percentage in most cases.

4. Discussion

All six simulations presented here produce cycle thickness distributions that are statistically indistinguishable from a stochastic Poisson process. This is despite there being no random process included in Carbonate GPM, and despite five of the six simulations being forced by a wide range of eustatic sea-level variations.

Using a variety of statistical techniques, both allocyclic and autocyclic signals could be detected. However, differentiating between the two is not trivial. To obtain sufficient confidence in the analysis a large number of cycles are required. Here, multiple vertical sections are included within a single analysis to ensure sufficient data availability, but in doing so along-shore variability is included in the analysis. Like Carbonate GPM, the model of Dexter et al. (2009) contained no random processes, but it was only two-dimensional and therefore could not include along-shore variability. Those authors attribute the exponential distribution of cycles to the complexity of the forcing signal that they imposed via eustatic sea level variations. By contrast, very simple (single or dual frequency) forcing is used here and exponential distributions of cycle thicknesses across the platform are still observed. We therefore conclude that along-shore variations in deposition rates are responsible for the overall exponential distribution.

The spectral analysis showed three main results: first if high quality data are available, such as those used to derive preserved water depth, then it is certainly possible to detect the forcing (allocyclic) signal, regardless of preservation percentage. Also, given a sufficient number of data, it is detectable above the autocyclic "noise." However, this result is dependent on the allocyclic frequency and amplitude. Second, in general, spectra derived from cycle thicknesses do not record the forcing frequencies. With these data alone and no prior knowledge of the external forcing signal it would be impossible to distinguish between auto- and allo-cyclic signals, especially considering that multiple autocyclic peaks occurred within the Milankovitch frequency band. Third, by increasing the period of the forcing frequency, the forcing signal is harder to detect using cycle thicknesses and moreover this makes lower amplitude signals more difficult to detect.

Unlike previous numerical forward models to study the distribution of cycle thicknesses (Dexter et al., 2009), Carbonate GPM is also capable of simulating autocycles without any randomness in the underlying processes as seen in the baseline simulation. Autocycles are manifest in a number of ways, including the introduction of spectral peaks at a wide range of frequencies which fall within the Milankovitch forcing frequencies expected from field studies. Hence, like previous models (Burgess, 2001, 2006) that can simulate autocycles, Carbonate GPM produces carbonate successions that contain Milankovitch-style signals, even where none were introduced, and moreover, the simulated stratigraphy may record any imposed forcing signals alongside the autocyclic signal. Without some prior knowledge of external forcing signals it would be impossible to distinguish between them. This result holds regardless of the data used to generate the power spectra, even if high quality data, such as accurately timed water depths, are available.

Carbonate GPM is a complex simulator, but it still lacks many processes such as tides, that will undoubtedly cause the results to differ from observed stratigraphies in the field. However, it is not currently feasible to include such processes when modelling geological timescales. This is a weakness in all numerical forward models to date. Nevertheless, our results and conclusions below are only likely to be reinforced if these processes were to be included, as they would be likely to add even more complexity to the stratigraphy, making recognition of eustatic forcing frequencies even more difficult.

Carbonate GPM is unique in that it is the only carbonate model that includes a proxy for calcium carbonate supersaturation. The lack of multiple facies within the shallow water areas makes cycle detection somewhat difficult in Carbonate GPM. A simple definition of a shallowing upwards cycle is used here, which may have some effect on the results presented here. However, our definition is similar to that of several other forward models from which sensible conclusions have been reached (Burgess and Emery, 2004; Burgess, 2008; Dexter et al., 2009), increasing confidence in the results.

5. Conclusions

Carbonate GPM is a numerical stratigraphic forward model capable of simulating realistic shallow-water carbonates (Hill et al., 2009). The simulations carried out here show a Poisson distribution as seen in many field studies (Wilkinson et al., 1998). This is true even with high amplitude eustatic forcing, and despite there being no random processes included in the model. From the model runs three time series can be derived from which the effect of preservation rates of the sediment can be assessed.

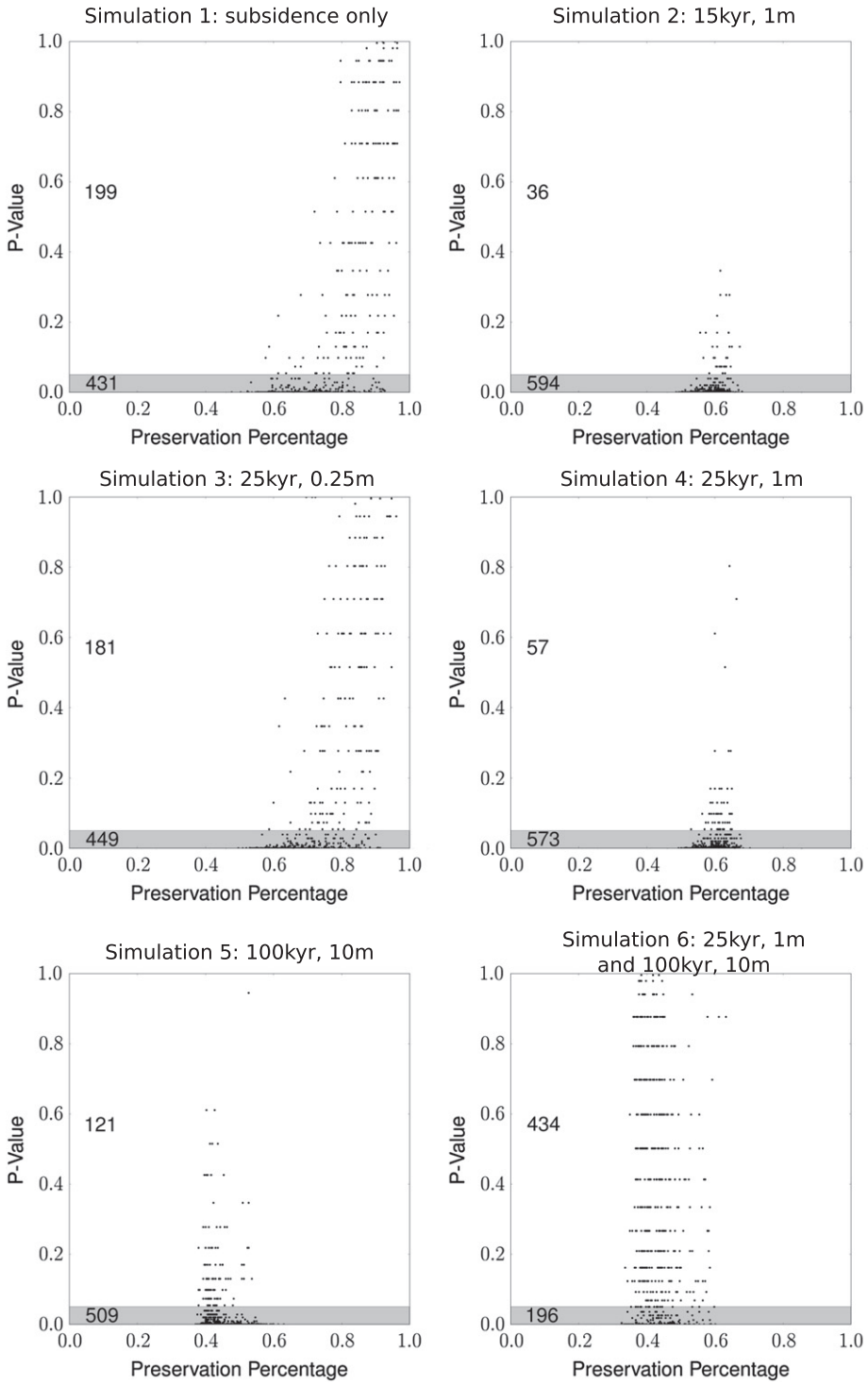

Fig. 10. *P*-value from a two-sample K–S test calculated from the true water depth spectra and the preserved water depth spectra, plotted against preservation percentage for each cell in the simulations (630 points). Horizontal grey band shows the 95% confidence interval that the two spectra are from the same distribution, such that points within this band are considered to have indistinguishable spectra. Numbers on the left-hand side above and within the grey band are the number of locations that show significant differences and those that do not, respectively.

Periodicity of eustatic variation is detectable in principle using an idealised reconstructed geological record, even with hiatal and erosional events. However, the signal is not reliably detectable using cycle thicknesses derived time series alone, which is often the only data measurable in the field. Autocyclic processes introduce "false" signals that are indistinguishable from the eustatic forcing frequencies without prior knowledge. The frequency and amplitude of the forcing signal affect whether the forcing signal is detectable in the preserved stratigraphy. Low amplitude signals are masked by autocyclic signals and low frequency signals are simply not preserved in the cycle thickness record. Moreover, lower frequency signals mask higher frequency signals.

Finally, preservation percentage appears to have little significant effect on the fidelity of the signal preserved. Although the higher quality

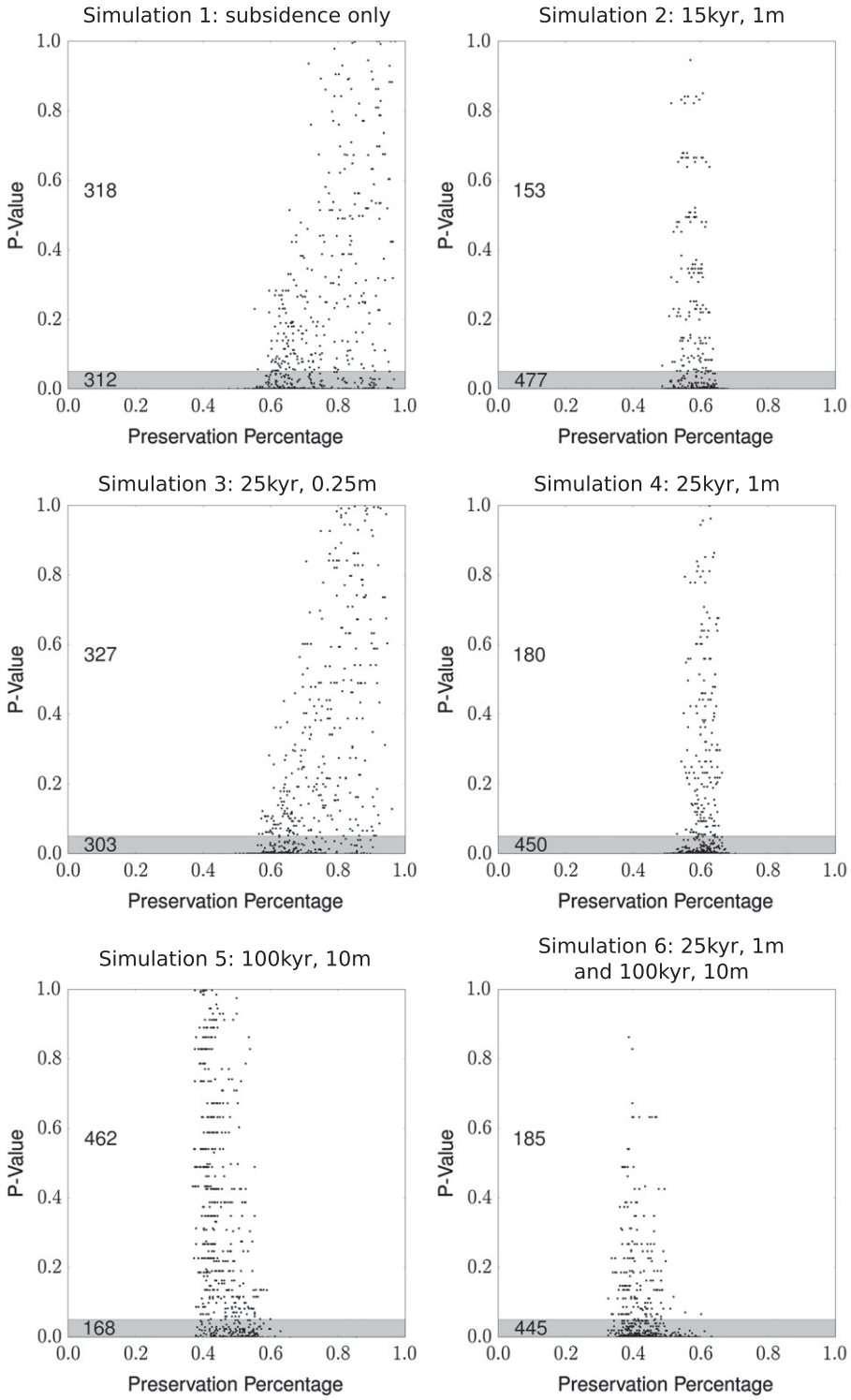

Fig. 11. *P*-value from a two-sample K–S test calculated from the true water depth spectra and the cycle thickness spectra, plotted against preservation percentage for each cell in the simulations (630 points). Horizontal grey band shows the 95% confidence interval that the two spectra are from the same distribution, such that points within this band are considered to have indistinguishable spectra. Numbers on the left-hand side above and within the grey band are the number of locations that show significant differences and those that do not, respectively.

preserved water depth derived spectra perform better than the cycle thickness derived spectra, the cycle thickness derived spectra still produce statistically significant matches to the true water depth derived spectra in 26–71% of vertical sections. Neither the preserved water depth derived spectra or the cycle thickness derived spectra show a significant trend between preservation rate and goodness of fit to the true water depth derived spectra. Vertical sections with preservation as low as 40% can still reliably detect both auto- and allo-cyclic forcing signals whilst sections with preservation as high as 90% may not preserve the signals accurately. The reverse of this is also true in other sections. It is therefore concluded that distinguishing allocyclic and autocyclic forcing from shallow marine carbonate geological sections is likely to be extremely difficult except in cases of extraordinary sedimentary preservation and dating accuracy.

Table 5
Number of locations where the null hypothesis of the power spectra generated from two data types are from the same distribution cannot be rejected with 95% confidence, from a total of 630 locations.

	Significant locations from K–S test	
Simulation	True:Pres.	True:Cycles
1	431 (68.41%)	312 (49.52%)
2	594 (94.29%)	477 (75.71%)
3	449 (71.27%)	303 (48.10%)
4	573 (90.95%)	450 (71.43%)
5	509 (80.79%)	168 (26.67%)
6	196 (31.11%)	445 (70.63%)

Acknowledgements

The research presented here, performed by Jon Hill as part of his doctoral work, was funded by the Natural Environment Research Council (Grant NER/S/C/2002/10583) and Schlumberger. The authors would like to thank an anonymous reviewer and Maurice Tucker for their reviews of the article.

References

Balog, A., Haas, J., Read, J.F., Coruh, C., 1997. Shallow marine record of orbitally forced cyclicity in a late Triassic carbonate platform, Hungary. Journal of Sedimentary Research 67, 661–675.
Barnett, A.J., Burgess, P.M., Wright, V.P., 2002. Icehouse world sea-level behaviour and resulting stratal patterns in late visean (Mississippian) carbonate platforms: integration of numerical forward modelling and outcrop studies. Basin Research 14, 417–438.
Bosence, D.W.J., Wood, J.L., Rose, E.P.F., Qing, H., 2000. Low- and high-frequency sea-level changes control peritidal carbonate cycles, facies and dolomitization in the Rock of Gibraltar (Early Jurassic, Iberian Peninsula). Journal of the Geological Society 157, 61–74.
Bosence, D., Procter, E., Aurell, M., Bel Kahla, A., Boudagher-Fadel, M., Casaglia, F., Cirilli, S., Mehdie, M., Nieto, L., Rey, J., Scherreiks, R., Soussi, M., Waltham, D., 2009. A dominant tectonic signal in high-frequency, peritidal carbonate cycles? A regional analysis of Liassic platforms from western Tethys. Journal of Sedimentary Research 79, 389–415.
Bosscher, H., Schlager, W., 1992. Computer simulation of reef growth. Sedimentology 39, 503–512.
Burgess, P.M., 2001. Modeling carbonate sequence development without relative sea-level oscillations. Geology 29, 1127–1130.
Burgess, P.M., 2006. The signal and the noise: forward modeling of allocyclic and autocyclic processes influencing peritidal carbonate stacking patterns. Journal of Sedimentary Research 76, 962–977.
Burgess, P.M., 2008. The nature of shallow-water carbonate lithofacies thickness distributions. Geology 36, 235–238.
Burgess, P.M., Emery, D.J., 2004. Sensitive dependence, divergence and unpredictable behaviour in a stratigraphic forward model of a carbonate system. In: Curtis, A., Wood, R. (Eds.), Geological Prior Information. : Special Publication, 239. Geological Society of London, London, p. 240.
Burgess, P.M., Pollitt, D.A., 2012. The origins of shallow-water carbonate lithofacies thickness distributions: one-dimensional forward modelling of relative sea-level and production rate control. Sedimentology 59, 57–80.
Burgess, P.M., Wright, V.P., 2003. Numerical forward modelling of carbonate platform dynamics: an evolution of complexity and completeness in carbonate strata. Journal of Sedimentary Research 73, 637–652.
Decisneros, C.J., Vera, J.A., 1993. Milankovitch cyclicity in Purbeck peritidal limestones of the Prebetic (Berriasian, Southern Spain). Sedimentology 40, 513–537.
Demicco, R.V., 1998. CYCOPATH 2D—a two-dimensional, forward model of cyclic sedimentation on carbonate platform. Computers & Geosciences 24, 405–423.
Demicco, R.V., Hardie, L.A., 2002. The "Carbonate Factory" revisited: a reexamination of sediment production functions used to model deposition on carbonate platforms. Journal of Sedimentary Research 72, 849–857.
Dexter, T.A., Kowalewski, M., Read, J.F., 2009. Distinguishing Milankovitch-driven processes in the rock record from stochasticity using computer-simulated stratigraphy. Journal of Geology 117, 349–361.
Drummond, C.N., Wilkinson, B.H., 1993. Aperiodic accumulation of cyclic peritidal carbonate. Geology 21, 1023–1026.
Drummond, C.N., Wilkinson, B.H., 1996. Stratal thickness frequencies and the prevalence of orderedness in stratigraphic sequences. Journal of Geology 104, 1–18.
Ginsburg, R.N., 1971. Landward movement of carbonate mud—new model for regressive cycles in carbonates. American Association of Petroleum Geologists Bulletin 55, 340.
Goldhammer, R.K., Dunn, P.A., Hardie, L.A., 1987. High frequency glacio-eustatic sealevel oscillations with Milankovitch characteristics recorded in the Middle Triassic platform carbonates in Northern Italy. American Journal of Science 287, 853–892.
Goldhammer, R.K., Dunn, P.A., Hardie, L.A., 1990. Depositional cycles, composite sea-level changes, cycle stacking patterns, and the hierarchy of stratigraphic forcing: examples from the alpine Triassic platform carbonates. GSA Bulletin 102, 535–562.
Goldhammer, R.K., Lehmann, P.J., Dunn, P.A., 1993. The origin of high-frequency platform carbonate cycles and 3rd-order sequences (Lower Ordovician El-Paso Gp, West Texas)—constraints from outcrop data and stratigraphic modeling. Journal of Sedimentary Petrology 63, 318–359.
Hill, J., Tetzlaff, D., Curtis, A., Wood, R., 2009. Modeling shallow marine carbonate depositional systems. Computers & Geosciences 35, 1862–1874.
Hinnov, L.A., Goldhammer, R.K., 1991. Spectral-analysis of the Middle Triassic Latemar Limestone. Journal of Sedimentary Petrology 61, 1173–1193.
Hofmann, A., Dirks, P., Jelsma, H.A., 2004. Shallowing-upward carbonate cycles in the Belingwe Greenstone Belt, Zimbabwe: a record of Archean sea-level oscillations. Journal of Sedimentary Research 74, 64–81.
Kay, S., Marple Jr., S.L., 1981. Spectrum analysis—a modern perspective. Proceedings of the IEEE 69, 1380–1419.
Pardo-Igzquiza, E., Rodriguez-Tovar, F.J., 2005. MAXENPER: a program for maximum entropy spectral estimation with assessment of statistical significance by the permutation test. Computers & Geosciences 31, 555–567.
Sadler, P.M., 1981. Sediment accumulation rates and the completeness of stratigraphic sections. Journal of Geology 89, 569–584.
Satterley, A.K., 1996. The interpretation of cyclic successions of the Middle and Upper Triassic of the Northern and Southern Alps. Earth-Science Reviews 40, 181–207.
Spalluto, L., 2011. Facies evolution and sequence chronostratigraphy of a mid-Cretaceous shallow-water carbonate succession of the Apulia Carbonate Platform from the northern Murge area (Apulia, southern Italy). Facies 1–20.
Spence, G.H., Tucker, M.E., 2007. A proposed integrated multi-signature model for peritidal cycles in carbonates. Journal of Sedimentary Research 77, 797–808.
Tetzlaff, D., Priddy, G., 2001. Sedimentary process modeling: from academia to industry. In: Merrian, D.F., Davis, J.C. (Eds.), Geologic Modeling and Simulation: Sedimentary Systems. Kluwer Academic/Plenum Publishers, New York, pp. 45–69.
Tucker, M., Garland, J., 2010. High-frequency cycles and their sequence stratigraphic context: orbital forcing and tectonic controls on Devonian cyclicity, Belgium. Geologica Belgica 13, 213–240.
Warrlich, G.M.D., Waltham, D.A., Bosence, D.W.J., 2002. Quantifying the sequence stratigraphy and drowning mechanisms of atolls using a new forward modelling program (CARBONATE 3D). Basin Research 14, 379–400.
Wheatcroft, R.A., 1990. Preservation potential of sedimentary event layers. Geology 18, 843–845.
Wilkinson, B.H., Diedrich, N.W., Drummond, C.N., 1996. Facies successions in peritidal carbonate sequences. Journal of Sedimentary Research 66, 1065–1078.
Wilkinson, B.H., Diedrich, N.W., Drummond, C.N., Rothman, E.D., 1998. Michigan hockey, meteoric precipitation, and rhythmicity of accumulation on peritidal carbonate platforms. Geological Society of America Bulletin 110, 1075–1093.
Wilkinson, B.H., Drummond, C.N., Diedrich, N.W., Rothman, E.D., 1999. Poisson processes of carbonate accumulation on Paleozoic and Holocene platforms. Journal of Sedimentary Research 69, 338–350.